

# Hosts and Alignment Effect in $0.5 < z < 1$ radio sources

Susan E. Ridgway

Astrophysics, NAPL  
University of Oxford  
Keble Rd  
Oxford OX1 3RH UK

## Abstract

*R*- and *I*- band images with good seeing at the NOT of the hosts of a sample of 7C radio galaxies at  $z \sim 0.7$  (with mean radio flux 20 times fainter than the 3C sample) show some evidence of radio-optical alignment. A quantitative analysis of the alignment in this sample and in a corresponding 3C sample from HST archival data indicates that the percentage of aligned flux may be lower and of smaller spatial scale in the faint radio sample. Studies of the aligned material in  $z \sim 1$  3C source hosts indicate that the quasar extensions also show some aligned flux, though much of it is due to optical synchrotron radiation.

## 1 Introduction

Studies of samples of high radio luminosity radio galaxies at  $z \geq 0.8$  show that the position angles of the optical and emission-line morphologies tend to align with the radio axis (McCarthy et al. 1987, Chambers et al. 1987). High-resolution optical imaging with the Hubble Space Telescope revealed that the aligned material is morphologically distributed in a wide variety of ways (e.g. Best et al. 1996, 1997), and is unlikely to be the result of a single mechanism. Apart from 3C368, in most objects nebular continuum fails to explain more than a fraction of the aligned light. Scattering of a hidden quasar nucleus is expected to add to the aligned light, and the detection of broad, polarised MgII emission in a number of these objects (e.g. 3C265 and 3C324; Dey & Spinrad

1996; Cimatti et al. 1996) proves that this must be an important contributor. The closely aligned morphologies seen in the WFPC2 imaging are inconsistent with pure scattering models, and star formation induced by the passage of the radio jet has been proposed by many (e.g. Chambers et al. 1990, Best et al. 1996, Dey et al. 1997).

How will the alignment effect depend on the radio power of the source sample? Some of these alignment mechanisms might be expected to result in a nearly linear dependence of the amount of aligned optical emission on the radio luminosity of the sources. The radio luminosity and the strength of narrow optical emission lines in radio galaxies are known to be well correlated (Rawlings et al. 1989). Recently, a correlation of the optical continuum luminosity of steep-spectrum radio-loud quasars with radio luminosity has also been established (Serjeant et al. 1998). Both of these imply a close relationship between the optical/UV luminosity of the AGN and the radio luminosity, presumably via a correlation with the bulk kinetic power of the radio jets (Rawlings & Saunders 1991).

Two imaging studies in the near-infrared, that of Dunlop & Peacock (1991) and of Eales et al. (1997), found that the “alignment effect” was unmeasurably small in samples of  $z \sim 1$  radio sources approximately ten and four times fainter than 3C respectively. Both these studies were, however, carried out under conditions of poor ( $> 1''$ ) seeing, and in the  $K$ -band, where the alignment effect is weak even in 3C (Rigler et al. 1991). They may not have been able to constrain how strongly the alignment effect depends on radio luminosity.

Here, I will discuss the result of a project done in collaboration with Mark Lacy at the University of Oxford to analyze alignments in a sample of low-luminosity radio sources ( $\sim 20$  times fainter than 3C) from the 7C North Ecliptic Cap (NEC) survey of Lacy et al. (1993). I will also discuss some of the alignments seen in 3C quasars at  $z \sim 1$ , based on a WFPC2 imaging project done in collaboration with Alan Stockton at the University of Hawaii.

## 2 Alignments in a 7C sample of radio galaxies

The 7C NEC sample of sources was selected to a flux limit of 0.5 Jy at 151 MHz, and has been spectroscopically identified to a completeness level of  $\sim 90\%$  (Lacy et al. 1993, Lacy et al. in prep). As a by-product of a project to study the clustering properties of a complete, extended (radio size  $\theta_r > 1''$ )  $0.5 < z < 0.82$  sub-sample of these 7C sources (Wold et al. 1996, Lacy this volume), fairly deep, high image quality  $I$  or  $R$ -band images of the radio galaxies

themselves were obtained. These images were 40 min exposures obtained at the 2.56 Nordic Optical Telescope (NOT) with seeing conditions ranging from  $0''.5$  to  $0''.9$ . Spectroscopy of all of these objects has been obtained with ISIS on the William Herschel Telescope (WHT) as part of the sample identification process, with slit positions generally along the radio axis.

A visual inspection of the images (Fig. 1) reveals a number of objects in which the optical morphology appears aligned with the radio axis. The morphologies of the aligned material differ: in two cases, the hosts are apparently ellipticals with the major axis within  $30^\circ$  of the radio PA, while others (e.g. 7C1748+6731 and 7C1826+6510) have multicomponent morphologies along the radio axis similar to that seen in the high luminosity 3C sources. However, in the ‘‘elliptical’’ host 7C1745+6415, the spectrum and consequently the morphology visible in the I-band image are dominated by emission lines rather than stellar continuum (Fig. 2). On the other hand, in 7C1826+6510, which has a secondary component  $d$  lying along the radio axis well-separated spatially from the host galaxy  $b$ , the spectrum of  $d$  confirms that it is probably associated. Its spectrum is dominated by stellar continuum and shows a  $4000\text{\AA}$  break and stellar absorption features with a  $\sim 8000$  km/sec velocity relative to the central component  $b$ . Furthermore, visible in the image is diffuse material lying along the radio axis.

Therefore, this moderate redshift, low luminosity sample of objects seems to have a number of cases of the alignment effect similar to that shown in the  $z \sim 1$  3C sources. To test whether this is a statistically significant result, we attempt to make a quantitative measurement of the ‘‘alignment effect’’ and compare these measurements to those derived for a sample of 3C galaxies in the same redshift range with imaging data available in the HST archive.

### 3 Quantitative Analysis of Alignment Effect

We have used two methods to measure the alignment of the galaxies in these samples: first, a standard moment analysis to derive the difference in the optical position angle from the radio position angle ( $\Delta$  PA) (Rigler et al. 1992, Dunlop & Peacock 1994, Ridgway & Stockton 1997), and second, a simple derivation of the percentage aligned flux, which should be less susceptible to skewing by companions and differences in observational resolution. To derive this % aligned flux, we have summed the flux within  $\pm 45^\circ$  of the lines joining the nucleus to each of the radio hotspots, and subtracted the remaining flux. We exclude from the sums the central portion of each galaxy within the FWHM of the seeing for the ground-based data, and for the archival HST data, we exclude

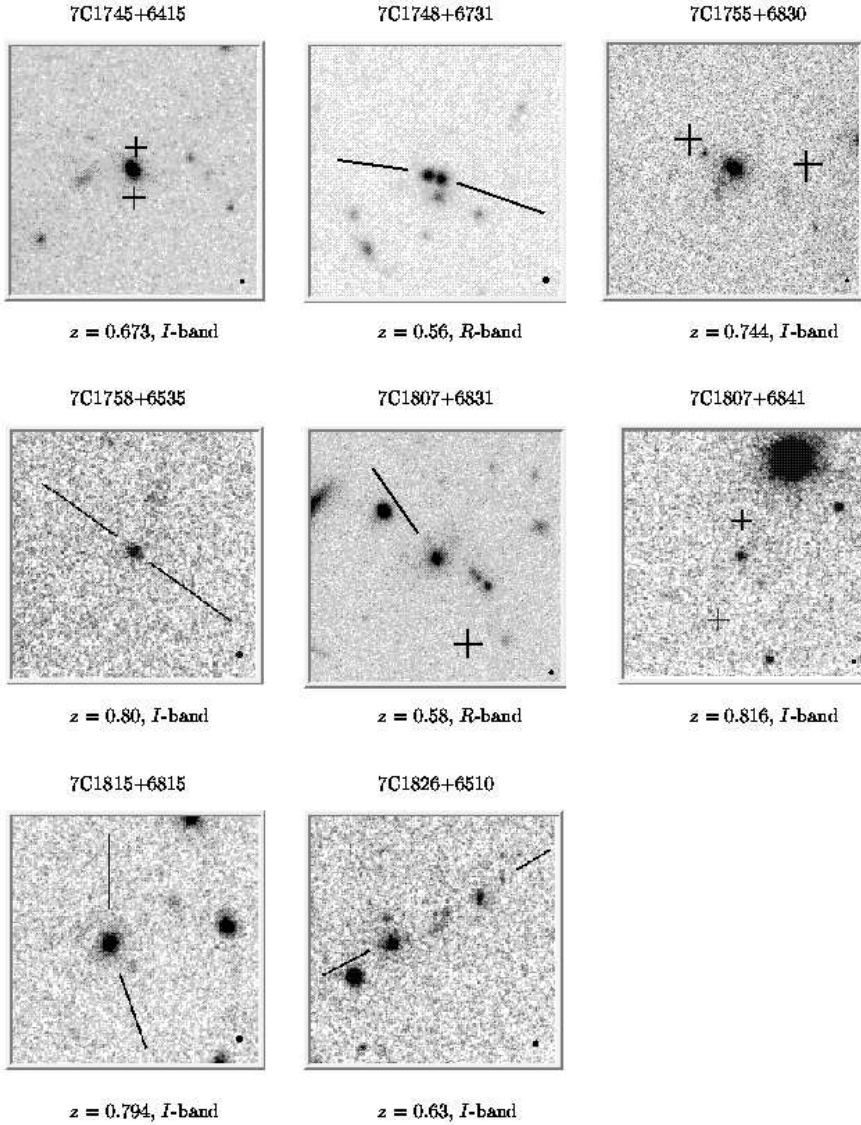


**Figure 1.** The 7C galaxies analyzed in this paper, with N up E left. The images are  $28''$  square. The black crosses designate the positions of radio hotspots, while the black lines show directions to the hot spots if they fall outside the field. The IDs are generally obvious, except in 7C 1826+6510 where it is the object *b* to the SE, marked with the radio lobe line. The aligned object *d* is marked by the other radio lobe directional line.

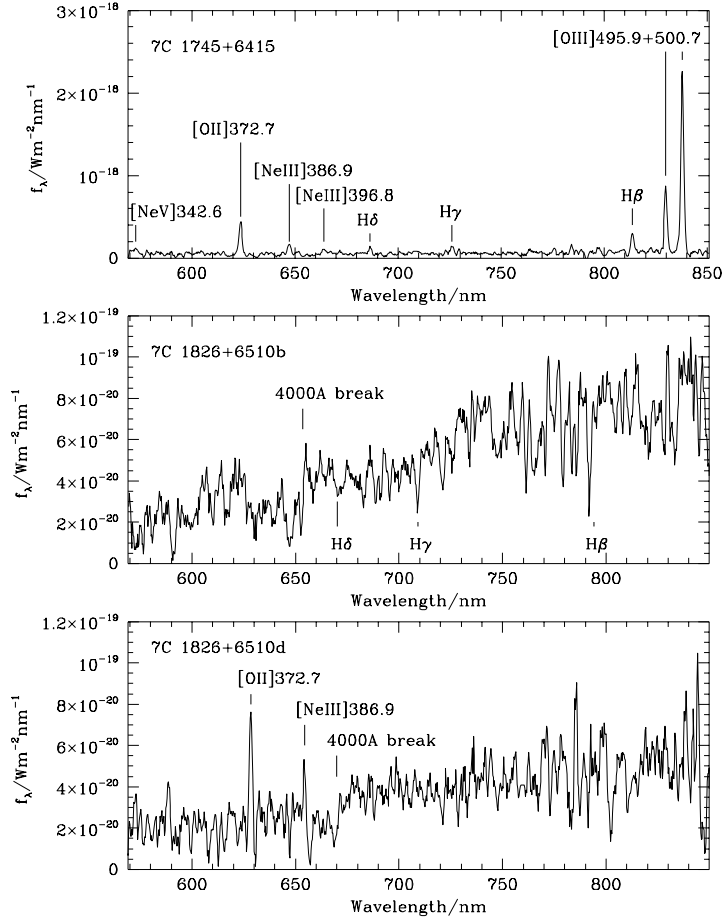


**Figure 2.** Top: WHT spectrum of 7C1745+6415. Middle: WHT spectrum of 7C 1826+6510 *b*, the radio source identification. Lower: WHT spectrum of 7C 1826+6510 *d*, an aligned object.

a circular region with a diameter ( $0''.5$ ) comparable to the FWHM of the best seeing ground-based images. This % aligned flux value will be positive for images with more flux within the cone of the radio axes than without, and will be negative for objects with more counter-aligned than aligned flux.

To make intercomparisons between objects in this fairly inhomeogenous dataset, we must account both for differences in the depth of the observations and the spread in redshift across the samples. Before analysis, we have therefore resampled the 7C NOT and 3C WFPC2 images to a common pixel scale, and then corrected the surface brightnesses for the differences in cosmological dimming by normalizing to the median redshift of the samples ( $z=0.7$ ) (by assuming that  $F_\lambda \propto (1+z)^{-5}$ , i.e. that the galaxies' intrinsic spectra are approximately flat in  $F_\lambda$  at these wavelengths).

A well-known problem with the standard position angle analysis is the subjectivity of choosing the isophotal cutoff level and the aperture within which to calculate the moments. In this paper, we have chosen a single isophotal cutoff, used for all the images, which is about 2.5 times the median normalized sky sigma in these frames for both the position angle analysis and for the % aligned flux analysis. Inspection of the behavior of the integrated % aligned flux in increasing apertures up to about  $10''$  showed that in general there were two spatial regions which tended to contain the major flux contributions: within about  $2''$  ( $\sim 15$  kpc) and within about  $6''$  ( $\sim 50$  kpc). This led us to choose 15 kpc and 50 kpc as the radii of our standard apertures for our analyses, calculated at the redshift of each object using  $H_0 = 50 \text{ km s}^{-1} \text{ Mpc}^{-1}$ ,  $q_0 = 0.5$ .

We therefore calculate for each object in the sample the  $\Delta\text{PA}$  and the % aligned flux as described above, within these two apertures after making the isophotal cutoff. For many of these objects, which were observed longer or were at lower than median redshift, this standard isophotal cutoff may result in losing obviously well-detected low surface brightness material: for example, large scale extended aligned material in 3C 277.2 falls below this cutoff. This is necessary, of course, to make the comparison on an unbiased basis. We have also calculated the % aligned flux in the annulus between 15 kpc and 50 kpc, and we give in Table 1 the results of these analyses for both samples. Also given are the unnormalized aperture magnitudes for the objects.

## 4 Results of Analysis

We give in Figures 3 and 4 histograms of the results of the  $\Delta\text{PA}$  and % aligned flux analysis within the 15 and 50 kpc apertures for the 7C and 3C samples. The

**Table 1.** Results of alignment analysis

Name	% Aligned Flux (15 kpc)	% Aligned Flux (50 kpc)	% Aligned Flux (15 – 50 kpc)	$\Delta$ PA (15 kpc)	$\Delta$ PA (50 kpc)	m(AB) (15kpc)	m(AB) (50 kpc)
3C34	$4.1 \pm 1$	$-44 \pm 1$	$-68.1 \pm 1$	20	73	20.0	19.7
3C41	$-6.9 \pm 1$	$16 \pm 1$	$96.3 \pm 3$	88	22	20.9	20.4
3C172	$10.6 \pm 1$	$37.2 \pm 1$	$44.8 \pm 1$	12	23	19.9	18.9
3C226	$24.8 \pm 1$	$17.1 \pm 1$	$-8.5 \pm 2$	2.7	36	20.9	20.3
3C228	$-9.9 \pm 2$	-	-	62	-	19.8	-
3C247	$-7.6 \pm 1$	$41.0 \pm 1$	$89.6 \pm 1$	74	14	20.2	19.1
3C265	$7.8 \pm 1$	$15.4 \pm 1$	$23.5 \pm 1$	19	11	20.1	19.3
3C277.2	$22.1 \pm 1$	$3.2 \pm 1$	$-90.0 \pm 1$	11	75	20.6	20.2
3C337	$25.2 \pm 1$	$55.4 \pm 1$	$79.7 \pm 1$	2.5	10	20.7	20.2
3C340	$15.8 \pm 1$	$19.4 \pm 1$	$92.9 \pm 7$	13	18	21.1	20.8
3C441	$18.6 \pm 1$	$27.5 \pm 1$	$33.8 \pm 1$	17	7	20.8	19.9
Median 3C	11	18	39	17	20	20.6	20.1
7C1745+6415	$6.5 \pm 1$	$6.5 \pm 1$	$0 \pm 0$	35	35	19.7	19.5
7C1748+6731	$100 \pm 2$	$100 \pm 2$	$0 \pm 0$	1.5	1.5	21.1	20.4
7C1755+6830	$12.2 \pm 1$	$8.8 \pm 1$	$-6.1 \pm 3$	22	4	21.0	20.5
7C1758+6535	$-3.7 \pm 7$	$-13.4 \pm 6$	$-47 \pm 15$	2	72	21.4	20.9
7C1807+6831	$15.1 \pm 1$	$24.4 \pm 1$	$81 \pm 4$	11	35	20.6	19.9
7C1807+6841	$-9.2 \pm 3$	$-11.5 \pm 2$	$-12.3 \pm 2$	17	70	21.6	-
7C1815+6815	$6.8 \pm 2$	$7.3 \pm 2$	$16.9 \pm 10$	28	25	20.2	19.7
7C1826+6510	$10.3 \pm 3$	$4.5 \pm 3$	$-11.9 \pm 6$	11	22	20.1	19.5
Median 7C	9	7	-6	14	30	20.8	19.9

(1) The errors given are the statistical errors based on the contribution of sky noise to each sum. (2) The “ $0 \pm 0$ ” values mean that no flux was left above the isophotal cutoff in those annuli. (3) The 3C 228 image was a very short single PC exposure; only the inner portion was used since all CRs were removed by hand.

**Table 2.** Summary of results of statistical tests

Number	Distributions tested	Type of Test	Result	Probability
1	7C $\Delta$ PA (15 kpc) vs. uniform	K.S. (One-sided)	D = 0.617	0.002
2	3C $\Delta$ PA (15 kpc) vs. uniform	K.S. (One-sided)	D = 0.505	0.004
3	7C $\Delta$ PA (50 kpc) vs. uniform	K.S. (One-sided)	D = 0.361	0.193
4	3C $\Delta$ PA (50 kpc) vs. uniform	K.S. (One-sided)	D = 0.444	0.026
5	% Align. Flux (15 kpc): 7C vs. 3C	K.S. (Two-sided)	D = 0.330	0.573
6	% Align. Flux (50 kpc): 7C vs. 3C	K.S. (Two-sided)	D = 0.550	0.095
7	% Align. Flux (15 – 50 kpc): 7C vs. 3C	K.S. (Two-sided)	D = 0.575	0.070
8	% Align. Flux (15 – 50 kpc): 7C vs. 3C	K.S. (One-sided)	D = 0.575	0.035

% aligned flux median values given in Table 1 seem to indicate a comparable degree of alignment in the 7C as in the 3C sample, at least at the 15 kpc radius. In the region between 15 kpc and 50 kpc, however, the 3C sample seems more aligned.

To determine whether these results indicate a significant alignment in the 7C and 3C samples, we have made a number of statistical tests, the results of which we give in Table 2. First we determine whether the  $\Delta$ PA values are consistent with random orientation; a Kolmogorov-Smirnov (K.S.) test of the values versus a uniform distribution (Table 2, lines 1 & 2) shows that at 15 kpc both the 7C and the 3C sample have a probability of less than 1% of being randomly oriented. The same test for the 50 kpc aperture is less conclusive for both samples, as might be expected from an increased slewing of the PA by companion objects, but particularly for the 7C sample (line 3).

What about the % aligned flux values? We have made a K.S. test to determine whether the 7C and 3C % aligned flux distributions differ significantly, and find that in the 15 kpc aperture, there is no significant difference (Table 2, line 5). Within the 50 kpc aperture, and particularly in the 15 – 50 kpc annulus, we find that the probabilities of having such different distributions by chance is significantly reduced (Table 2, lines 6,7,8).

From these tests we can conclude that at least at the 15 kpc scale the 7C sample we have observed seems to exhibit a significant alignment effect. At the larger 50 kpc scale, while the 3C sample continues to show a similar or perhaps increasing amount of aligned flux, the 7C sample is less well aligned.



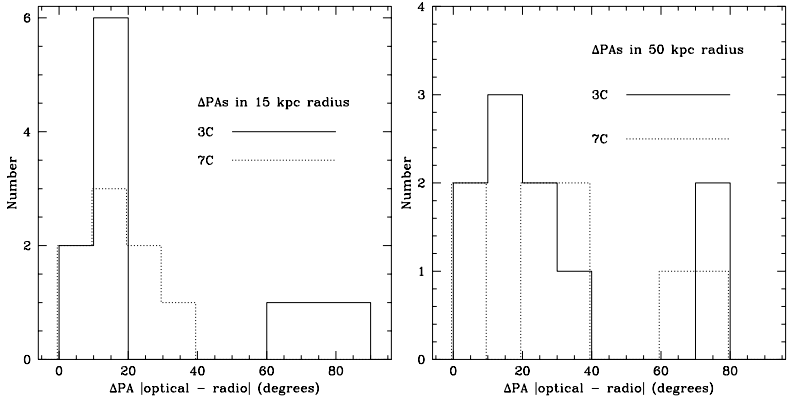


**Figure 3.** Left:  $\Delta$ PAs (difference between the optical and radio axes) for the 3C and 7C galaxies within the 15 kpc aperture. Right:  $\Delta$ PAs for the two samples within the 50 kpc aperture.

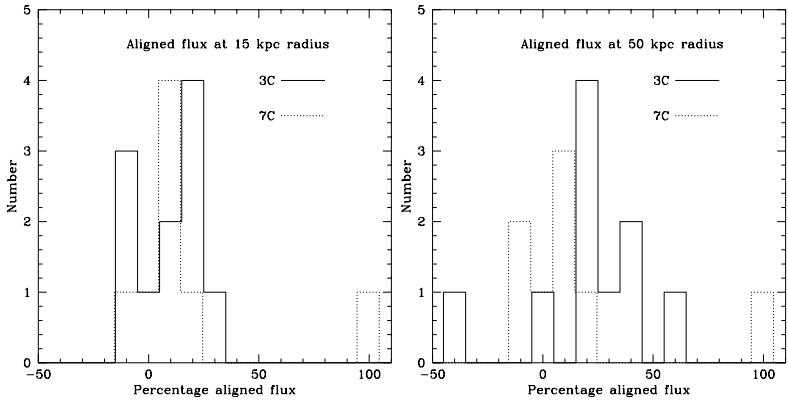


**Figure 4.** Left: Aligned flux percentage for the 3C and 7C galaxies within the 15 kpc aperture. Right: Aligned flux percentages for the two samples within the 50 kpc aperture.

## 5 Discussion

Though these results are admittedly based on small samples and are not of great statistical significance, they are quite suggestive. We seem to have significant alignment at a 15 kpc scale in a sample of radio galaxies whose luminosity is  $\sim 20$  times fainter than that of the 3C sample.

Two of the most common alignment mechanisms known to operate in the 3C sample are scattering and nebular continuum emission. Both of these should scale approximately as the emission line strengths, which are found to scale approximately with the radio luminosity (to about the 6/7 power; Rawlings & Saunders 1991). We should therefore expect contributions from scattering and nebular continuum emission to be about a factor of 15 less in the 7C sample than in the 3C sample; were the percentage alignments this much diminished they would have been undetectable. The probable luminosity dependence of other mechanisms are less clear, but may scale less severely with radio power. Jet-induced star formation is not well understood, but could in theory be more effective with lower jet velocities, and the “selection bias” effect of Eales (1992) might also operate effectively in low radio luminosity samples.

Of course, even if we are correct in finding almost comparable percentage alignments in the 7C sample and the 3C sample at  $\sim 15$  kpc, this does not necessarily translate into ascribing the same alignment mechanism to the two samples. An important difference seems to be in the scale of the aligned material.

We have shown that in this sample, the 3C objects are aligned over a large range in scales. In the extensively studied  $z \sim 1$  3C galaxies, of which these are probably a reasonably typical subset (though at slightly lower  $z$ ), it is known that there is a variety of causes for the alignment effect, some of which would work fairly well at large scales, such as scattering. In our 3C sample, some galaxies such as 3C 265 have been studied with ground-based polarimetry and are known to be quite polarized, and therefore probably have a large scattering contribution to the aligned light. Though we do not have in our 3C sample any obvious examples in which the very small scale, “jet path” aligned morphology (e.g. 3C 324) dominates, this is probably due to the more dominant elliptical hosts at longer rest wavelengths, and this very small scale alignment mechanism may still be contributing. We can probably assume that in this sample the same wide range of mechanisms determined in the  $z \sim 1$  samples are contributing, and some of these mechanisms are obviously effective at scales of  $\sim 50$  kpc.

Why, then, are the galaxies in this 7C sample aligned? First, we find that the alignment is comparable to that of the 3C sample at scales of  $\sim 15$  kpc, but probably not at the larger scales of  $\sim 50$  kpc. We have no information, of course,

at the very small ( $0''.1$ ) scale at which some 3C objects show alignment. Our result, though reasonably good statistically, is based on a few objects, which show a fair bit of variation in type of aligned morphology themselves. So it is difficult to tell what the likely mechanisms are, and why they do not seem to be operating at  $\sim 50$  kpc scales.

Some possible explanations for the scale difference are that the alignment mechanisms that operate at the large scales in the 3C are the most luminosity dependent, such as scattering or nebular continuum. In addition, there may simply be less material at larger scales in the 7C environments to be aligned or to act as a scattering medium. (We do find on average, with great dispersion, twice as much flux above the isophotal cutoff in the 3C as in the 7C in the 15 – 50 kpc annulus).

Nevertheless, the alignment that we seem to see in the 7C sample indicates that some less-luminosity dependent alignment mechanism, effective at moderately small scales, may be contributing to the “alignment effect” that we see in radio sources. That the 3C alignments extend to larger scales could mean that this less-luminosity dependent alignment mechanism is swamped by other effects, such as scattering, in the more powerful radio sources. We will discuss these results in more detail in Lacy et al. (1998).

## 6 Alignment effect in 3CR Quasars

What about the other type of radio source, the quasars? In a WFPC2 project to study a sample of  $z \sim 1$  3CR sources, Alan Stockton and I obtained  $\sim R$  images of 5 steep-spectrum quasars with extended radio structures (Ridgway & Stockton 1997). We were able to resolve circumnuclear optical emission in all 5 of the quasars, and found that in 4 cases the optical structures were aligned closely with the radio structure. In one quasar, 3C 196, the type of aligned morphology is similar to that seen in the 3C galaxies. In the other three, the morphological correspondence between the optical and radio is so close that it is almost certainly optical synchrotron emission or similar non-thermal process. 3C 2 has an optical synchrotron northern lobe/hot spot, while the other two, 3C 212 and 3C 245, both have optical synchrotron jets. We have been obtaining high-resolution MERLIN mapping of the sources, which has allowed us to determine radio-optical spectral indices for many of the components unresolvable with previous radio mapping. In Fig. 5, we show the WFPC2 image of 3C 212 with an L band MERLIN map overlaid, and in Fig. 6 we show the derived SEDs for the various components. We find that the spectral indices and prob-

able turnovers are typical of those seen in lower  $z$  cases of optical synchrotron where the synchrotron nature has been proved with optical polarimetry. That we saw optical synchrotron in 3/5 quasars and 0/5 galaxies in this small sample is consistent with beaming and the unification hypothesis of AGNs.

## References

- Best P.N., Longair M.S., Röttgering H.J.A., 1996, MNRAS, 280, L9  
Best, P.N., Longair, M.S., & Röttgering, H.J.A. 1997, astro-ph/9707337  
Chambers, K.C., Miley, G., & van Breugel, W. 1987, Nature, 329, 609  
Chambers, K.C., Miley, G., & van Breugel, W. 1990, ApJ, 363, 21  
Cimatti A., Dey A., van Breugel W., Antonucci R., Spinrad H., 1996, ApJ, 145, 156  
Dey A., Spinrad H., 1996, ApJ, 459, 133  
Dey, A., van Breugel, W., Vacca, W., Antonucci, R. 1997, ApJ, 490, 698  
Dunlop, J., & Peacock, J. 1993, MNRAS, 263, 936  
Eales, S.A. 1992, ApJ, 397, 49.  
Lacy, M., Hill, G., Kaiser, M., & Rawlings, S. 1993, MNRAS, 263, 707  
Lacy, M., Ridgway, S.E., Wold, M., & Rawlings, S. 1998, MNRAS, submitted.  
McCarthy, P.J., van Breugel, W., Spinrad, H., & Djorgovski, S. 1987, ApJ, 321, L29  
Rawlings, S., & Saunders, R. 1991, 349, 148  
Rawling, S., Saunders, R., Eales, S.A. & Mackay, C.D. 1989, 240, 701.  
Ridgway, S.E., & Stockton, A. 1997, AJ, 114, 511  
Serjeant, S., Rawlings, S., Maddox, S.J., Baker, J.C., Clements, D., Lacy, M. & Lilje, P.B. 1998, MNRAS, 294, 494  
Wold M., 1996, Cand. Sci. thesis, University of Oslo

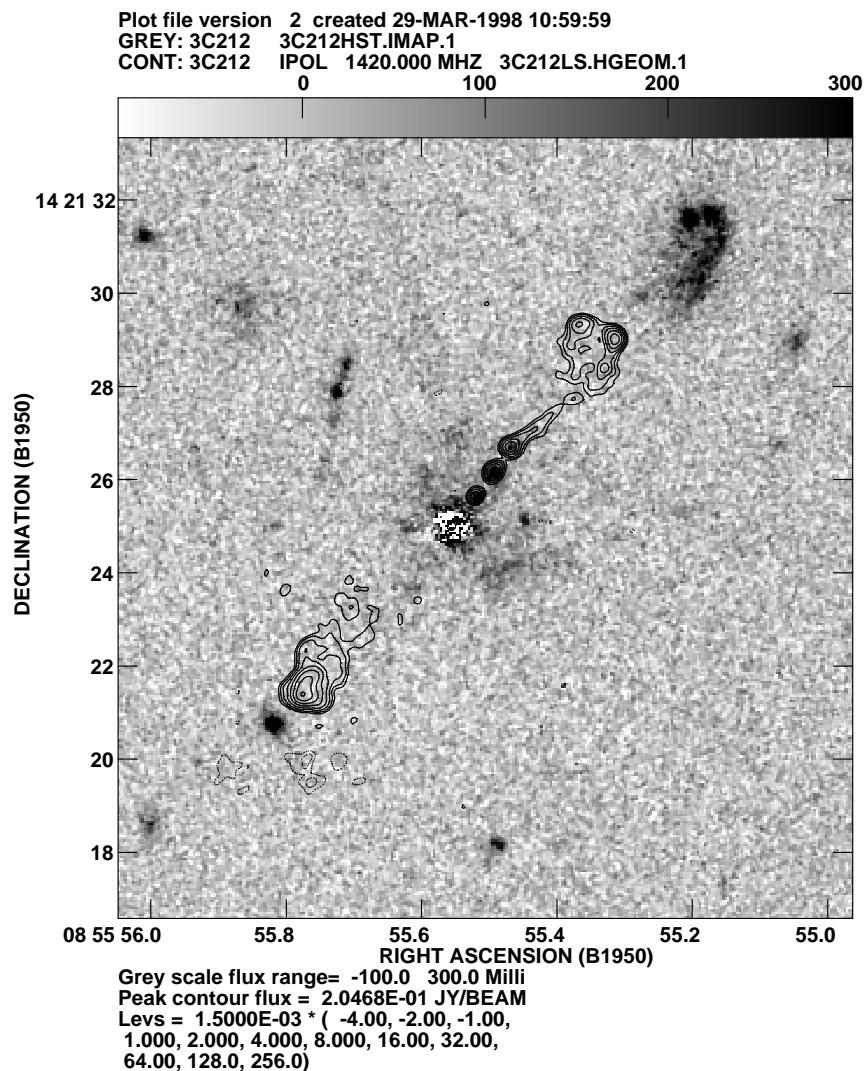


**Figure 5.** WFPC2 image of 3C 212, with the nucleus PSF-subtracted, and with MERLIN L band map overlaid. The three optical jet components lie to the NW of the nucleus, and correspond exactly in position to the radio jet knots seen in the MERLIN image. They are referred to as *a*, *b* and *c* in increasing distance from the core.

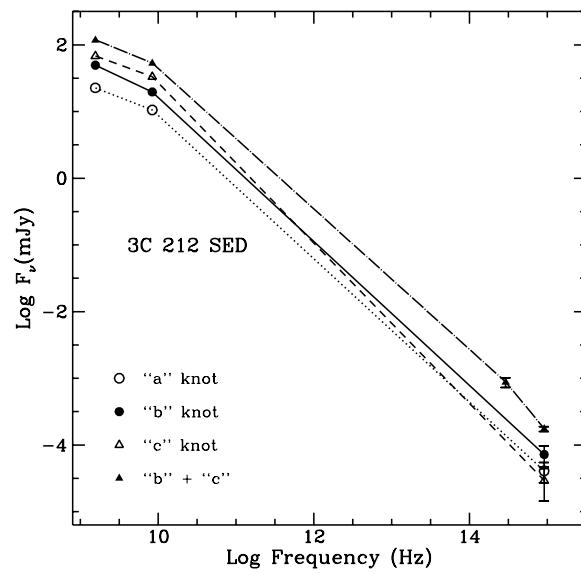


**Figure 6.** The spectral energy distributions of the jet components from the WFPC2 image, the MERLIN L band map, a VLA X band image, and from a Keck *K* band image (which was only able to resolve the sum of the outer two components,  $b + c$ ).